

Received: 2018.09.10

Accepted: 2018.11.21

Published: 2018.12.08

Abnormal DNA Methylation in Thoracic Spinal Cord Tissue Following Transection Injury

Authors' Contribution:
Study Design A
Data Collection B
Statistical Analysis C
Data Interpretation D
Manuscript Preparation E
Literature Search F
Funds Collection G

ABCEF 1,2 **Gui-Dong Shi***
ABCE 1,2 **Xiao-Lei Zhang***
B 1,2 **Xin Cheng**
BD 1,2 **Xu Wang**
AC 1,2 **Bao-You Fan**
CF 1,2 **Shen Liu**
CF 1,2 **Yan Hao**
CDF 1,2 **Zhi-Jian Wei**
BFG 1,2 **Xian-Hu Zhou**
BFG 1,2 **Shi-Qing Feng**

1 Department of Orthopedics, Tianjin Medical University General Hospital, Tianjin, P.R. China

2 Tianjin Neurological Institute, Key Laboratory of Post-Neuroinjury Neuro-Repair and Regeneration in Central Nervous System, Ministry of Education and Tianjin City, Tianjin, P.R. China

* Gui-Dong Shi and Xiao-Lei Zhang contributed equally

Corresponding Authors:

Source of support:

Xian-Hu Zhou, e-mail: zhouxh007@126.com, Shi-Qing Feng, e-mail: sqfeng@tmu.edu.cn

This study was supported by grants from the State Key Program of National Natural Science Foundation of China (81330042); Special Program for Sino-Russian Joint Research Sponsored by the Ministry of Science and Technology (2014DFR31210); International Cooperation Program of National Natural Science Foundation of China (81620108018); State General Program National Natural Science Foundation of China (81371957); and the Key Program Sponsored by the Tianjin Science and Technology Committee, China (14ZCZDSY00044, 13RCGFSY19000)

Background: Spinal cord injury (SCI) is a serious disease with high disability and mortality rates, with no effective therapeutic strategies available. In SCI, abnormal DNA methylation is considered to be associated with axonal regeneration and cell proliferation. However, the roles of key genes in potential molecular mechanisms of SCI are not clear.

Material/Methods: Subacute spinal cord injury models were established in Wistar rats. Histological observations and motor function assessments were performed separately. Whole-genome bisulfite sequencing (WGBS) was used to detect the methylation of genes. Gene ontology (GO) term enrichment and Kyoto Encyclopedia of Genes and Genomes (KEGG) pathway analysis were performed using the DAVID database. Protein-protein interaction (PPI) networks were analyzed by Cytoscape software.

Results: After SCI, many cavities, areas of necrotic tissue, and many inflammatory cells were observed, and motor function scores were low. After the whole-genome bisulfite sequencing, approximately 96 DMGs were screened, of which 50 were hypermethylated genes and 46 were hypomethylated genes. KEGG pathway analysis highlighted the Axon Guidance pathway, Endocytosis pathway, T cell receptor signaling pathway, and Hippo signaling pathway. Expression patterns of hypermethylated genes and hypomethylated genes detected by qRT-PCR were the opposite of WGBS data, and the difference was significant.

Conclusions: Abnormal methylated genes and key signaling pathways involved in spinal cord injury were identified through histological observation, behavioral assessment, and bioinformatics analysis. This research can serve as a source of additional information to expand understanding of spinal cord-induced epigenetic changes.

MeSH Keywords: **DNA Methylation • Epigenomics • Nerve Regeneration • Spinal Cord Injuries**

Full-text PDF: <https://www.medscimonit.com/abstract/index/idArt/913141>

 2838

 6

 5

 44



Background

Spinal cord injury (SCI) can lead to severe autonomic, sensory, and motor dysfunction [1]. It is estimated that more than 3 million people live with spinal cord injury and its worldwide incidence is 23 to 70 individuals per million [2]. Due to the high incidence and high disability rate of spinal cord injury, a serious burden has been placed on society and families. Spinal cord injury can be divided into primary mechanical injury and secondary injury [3]. According to the pathogenesis and the time after injury, the secondary injury process can be divided into acute, subacute, and chronic phases [4]. In addition, 'microenvironment imbalance' is considered to be the main cause of the poor regeneration and recovery of SCI [5]. Microenvironmental imbalances are often accompanied by increased inhibitory factors, loss of neurons, filling of glial cells and reduction of promoting factors at different times and spaces [6]. Multiple cells combined with different nutritional factors or scaffolds have become the focus of spinal cord injury repair [7]. However, treatment with cells, surgery, or medication have been unable to completely cure spinal cord injuries [8].

Conrad Waddington defined the term "epigenetics" to describe inherited changes in phenotypes without genotypic changes [9,10]. At present, epigenetics usually refers to a stable genetic phenotype resulting from a chromosome change without variations in the DNA sequence [11]. Due to the role of transcriptional and epigenetic regulations, even though mature cells start off with the same genotype, their phenotypes may quite different [12]. In the brain of adult vertebrates, the formation of new neurons occurs in a specific population of cells. Nerve regeneration is extremely difficult under normal physiological conditions, and it is usually described as being induced after spinal cord injury [13]. Although the exact mechanism of neural repair is not yet clear, previous studies have shown that specific cytoplasmatic factors (exosome), transcriptional factor network, and epigenetic regulators play key roles in nerve regeneration [14].

DNA methylation is one of the most thoroughly studied epigenetic modifications [15]. The characteristic of DNA methylation is adding a methyl group to cytosine nucleotide without changing the properties of base pairs. Due to the influence of environment or age, different DNA methylation patterns affect the expression of genes involved in crosstalk between neural activity and inflammatory pathways, further contributing to various diseases [16]. Previous studies have confirmed that DNA methylation is associated with a variety of diseases such as cancer [17], Alzheimer's disease [18], and hematological diseases [19]. DNA methyltransferases are key enzymes in the process of DNA methylation. More and more studies have shown that DNA methyltransferase plays a critical role in the early development of the central nervous system (CNS), including cognition,

learning, and memory [20]. However, the effect of DNA methylation on spinal cord injury has been unclear.

In the present study, whole-genome bisulfite sequencing (WGBS) technology was used to assess tissue before and after spinal cord transection in rats. The discovery of abnormal DNA methylation in the thoracic spinal cord might provide a new repair approach for epigenetic therapies of spinal cord injury.

Material and Methods

Animals

Adult female Wistar rats (approximately 230–250 g, provided by Radiation Study Institute-Animal Center, Tianjin, China, License Key: SCXK2012-0004) were used in this study. Two experimental groups were established: a sham group (n=9) and a SCI group (n=9). All animal experiments were performed according to the guidelines for laboratory animal safety and care as issued by the Ethics Committee of Tianjin Medical University General Hospital and the National Institutes of Health guide for the care and use of laboratory animals (NIH Publications No. 8023, revised 1978). All procedures performed in the study involving animals were consistent with the ethical standards set by the above-mentioned institutions.

Spinal cord transection

Adult female Wistar rats were used for spinal cord transection as described earlier [21–23]. In brief, all rats subjected to SCI were deeply anesthetized with isoflurane to minimize suffering. Following laminectomy at the T10–11 vertebral level, a 2-mm segment of spinal cord with associated spinal roots was completely removed at the T10 spinal cord level. Sham control rats also underwent laminectomy without contusion. For postoperative care, the bladder was emptied manually twice a day for a month. All rats received an intramuscular injection of penicillin (40 000 U/kg/day) for 5 days to prevent infection.

DNA methylation analysis

DNA was extracted from the spinal cord using a DNA extraction kit (TIANamp Genomic DNA Kit, China) according to the manufacturer's instructions. Five hundred nanograms of bisulfite-converted DNA per sample were analyzed by Illumina Infinium Human Methylation 450 BeadChip array (Illumina, China). Raw data analysis and preliminary data quality control were performed with GenomeStudio software 2011.1 (Illumina, China). Specific experimental procedures for DNA methylation sequencing are shown in Figure 1. For further gene expression analysis, all data were imported into Cytoscape software (v3.6.1) and GraphPad Prism software (Graph Pad v6.01) for functional

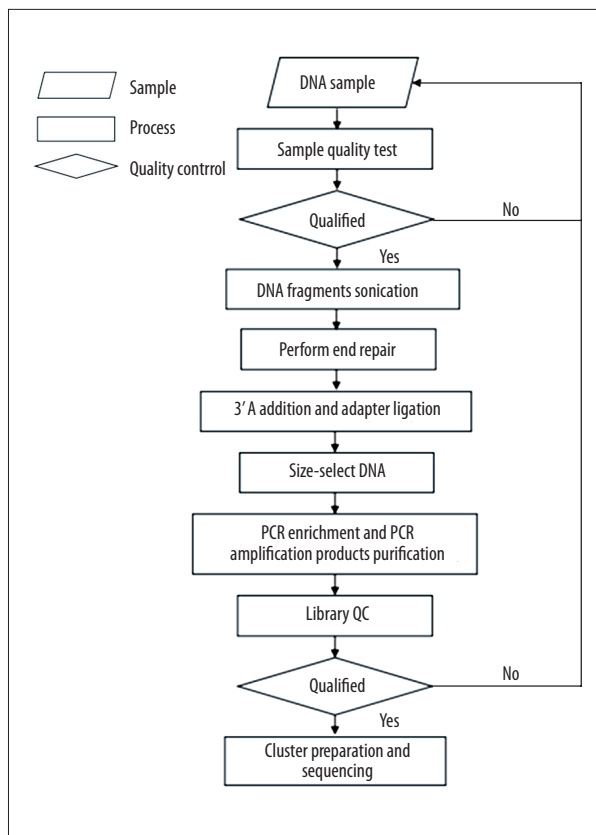


Figure 1. Concise experimental procedure for the whole-genome bisulfite sequencing.

analysis and statistical analysis [24]. Differentially methylated genes (DMGs) were identified (mean methylation difference ≥ 20 , $P < 0.001$) as described earlier [25]. Using the bioinformatics resources of DAVID 6.7 (<https://david.ncifcrf.gov/>), the Gene Ontology (GO) term enrichment and Kyoto Encyclopedia of Genes and Genomes (KEGG) pathway analysis of differentially methylated genes were performed [26].

Histology and immunohistochemistry

The histological evaluation was performed at 4 weeks post surgeries. The rats were anesthetized with isoflurane and transcardially perfused with 4% paraformaldehyde in PBS. Spinal cord tissue was cut into paraffin sagittal sections of 7 μm thickness. After the paraffin sections were prepared, the paraffin sections were stained with hematoxylin-eosin (Solarbio, China), as described previously [27]. Finally, the stained sections were observed under a microscope (Nikon, Japan).

Quantitative real-time PCR

Total RNA was extracted from spinal cord tissues using TRIzol reagent (Invitrogen, USA) according to the manufacturer's instructions [28]. One microgram of total RNA per sample was reverse-transcribed using a Reverse Transcription Kit (Applied Biosystems, USA). Quantitative real-time RT-PCR was performed on a LightCycler[®] 480 Real-Time PCR System (Roche, Germany) using SYBR-Green (Thermal, USA). GAPDH acted as internal control. The primers are listed in Table 1. All samples were analyzed in duplicate, then the average value of the duplicates was used for quantification.

Behavioral analysis

After surgery, hindlimb function of the rats was evaluated with the Basso, Beattie, and Bresnahan (BBB) open field locomotor test [29]. BBB scores were taken 3 days prior to injury, and once each week following SCI, for 8 weeks. BBB scores of each animal were calculated as the average of movement scores between the 2 hind limbs. Two independent researchers blind of the different experimental treatments determined the BBB scores.

Statistical analysis

All statistical analyses were performed using the GraphPad Prism software. Data are reported as mean \pm standard deviations. The BBB scores data were evaluated using 2-way

Table 1. Information on primer sequences.

Gene	Forward primer 5' to 3'	Reverse primer 5' to 3'	Annealing temperature (°C)
Csf2	AATGACATGCGTGCTCTGGAGAAC	TCGTCTGGTAGTGGCTGGCTATC	54
Fars2	CCACCTGGCAGAACTTCGATAGC	GTCACGCCGATACACATCACCTAC	54
Synj2	TCCATGTCTCGTACCATCCAGTCC	CCGTGTTGTCCAGCAGCATCC	53
Ppp3cc	TCCGAGGCTGCTCCTACTTCTTC	AGCCAGTTGCTTGGTTCTTCTG	54
Stat4	CAGGACTGGAAGAAGCGGCAAC	AAGCAGTTCTGAAGCTGGTCCAAC	53
Pcsk2	CACAGTCAACGCAACCAGGAGAG	ACCTGGAGTCGTCGTCTTGG	54
Dnm3	GTACACCCAGCCAACCCGATC	GGTGATAACCCAATGGTCTCAG	54
Hmgcl1	ACTCCAGGCAGCATGAAGACAATG	TCATGGCAGTGAACAGCAAGAGC	54

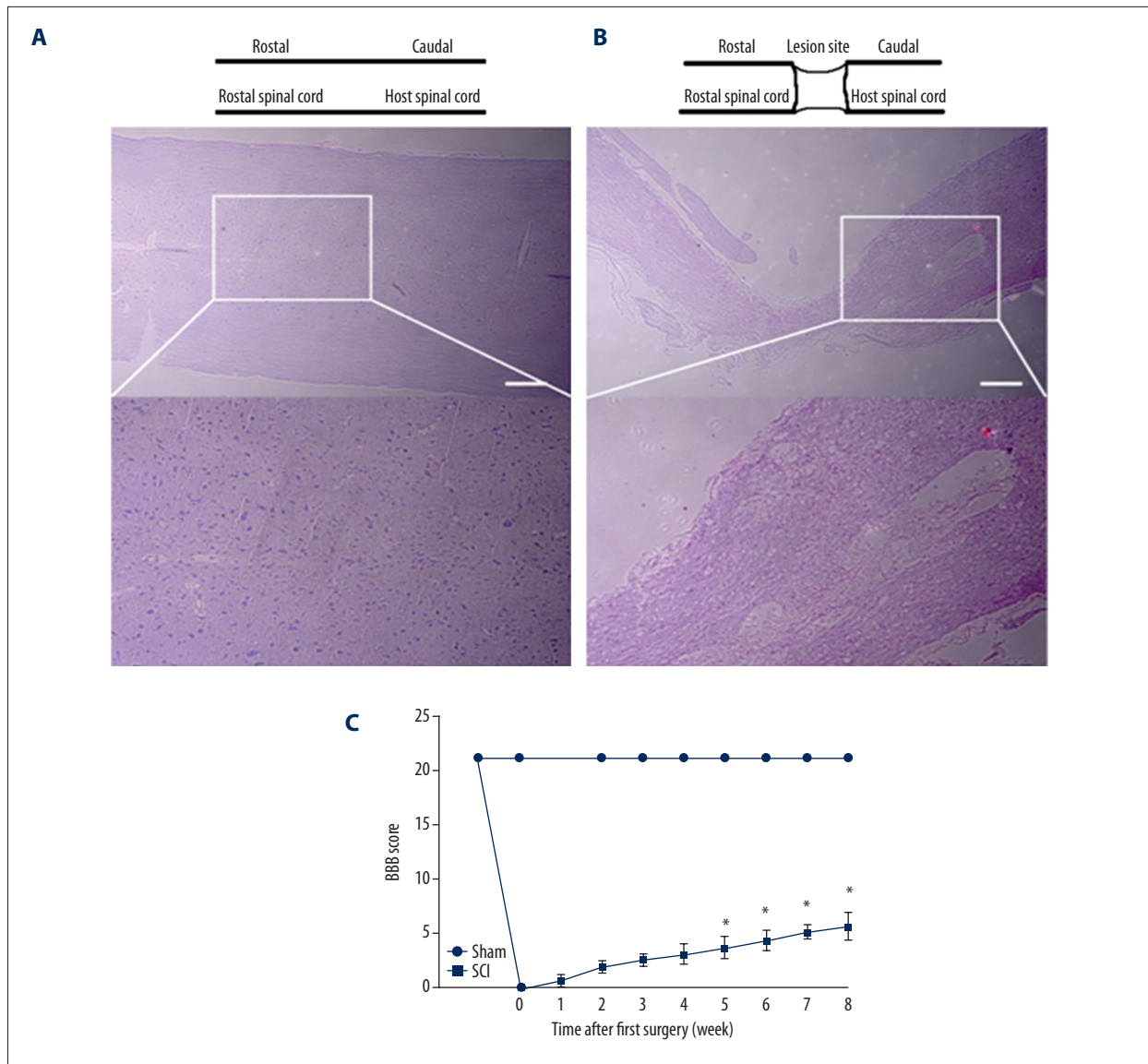


Figure 2. Histological observation and motor function assessment after spinal cord injury. **(A)** Hematoxylin-eosin staining of spinal cord sections in the sham group at 8 weeks after reperfusion. **(B)** Hematoxylin-eosin staining of spinal cord sections in the SCI group at 8 weeks after reperfusion. **(C)** BBB scores of Wistar rats. Values are means \pm SE (* $P < 0.0001$).

analysis of variance (ANOVA). $P < 0.05$ was considered a statistically significant difference.

Results

Histological and behavioral evaluation after spinal cord injury

After spinal cord injury, the loss of neuronal cell was noticeable and axons were severed. Cells and tissue morphology of the sham group were relatively complete (Figure 2A). Inflammatory cell infiltration, bleeding, and glial scars were observed in the

SCI group (Figure 2B). Motor function recovery was evaluated using the BBB open field locomotor test. The BBB scores ranged from 0 (no hindlimb movement) to 21 (normal hindlimb move) according to the rating scale. After successful spinal cord injury, the BBB score of all rats in the SCI group was 0. After 8 weeks, the score of motor function of some rats in the SCI group reached 5 (Figure 2C).

Identification of DMGs in SCI

After the whole-genome bisulfite sequencing, a total of 623 487 210 clean reads in the sham group and 623 545 728 clean reads in the SCI group were obtained, respectively. There were

Table 2. Differential methylation in the spinal cord.

Class	Hypermethylated	Hypomethylated	Total
Differentially methylated genes	590	568	1158 (100%)
DMG, $P < 0.05$, mean.meth.diff=20	189	181	370 (31.95%)
DMG, $P < 0.001$, mean.meth.diff=20 (remove repetition)	50	46	96 (8.29%)

1158 differentially methylated genes identified (Table 2). Among differentially methylated genes, 50.95% were hypermethylated and 49.05% were hypomethylated. A total of 370 differentially methylated genes between the sham group and SCI group were selected ($P < 0.05$). According to screening criteria (mean methylation difference ≥ 20 , $P < 0.001$), 96 methylated genes were selected. Among them, 50 genes were hypermethylated and 46 genes were hypomethylated (Tables 3, 4). All of the aberrantly expressed genes are shown in a heat map in Figure 3.

GO enrichment analysis and KEGG pathway analysis

The results of GO enrichment analysis are presented in Table 5. In the biological processes (BP), the hypermethylated genes were significantly enriched in spermatogenesis, regulation of cell shape, and neurogenesis. Regarding the molecular function (MF), the hypermethylated genes were mainly enriched in plasma protein binding and metal ion binding. In the cellular component (CC), the hypermethylated genes were significantly enriched in membrane, extracellular exosome, and membrane. The biological processes enriched by the hypomethylated genes included brain development, protein phosphorylation, and response to ethanol. In molecular function, the hypomethylated genes were mainly enriched in protein binding and calcium ion binding. In the cellular component, the hypomethylated genes were enriched in cytoplasm and extracellular exosome.

KEGG pathway analysis results are shown in Table 6. According to KEGG pathway analysis, the DMGs were significantly enriched in the Axon guidance pathway, Endocytosis pathway, T cell receptor signaling pathway, and Hippo signaling pathway.

PPI network analysis

Protein-protein interaction (PPI) networks analysis was performed using Cytoscape software. The PPI network of hypermethylated/hypomethylated genes is shown in Figure 4. According to Figure 4A, a total of 48 nodes and 41 interaction pairs were included in this network. Some proteins involved in the Calcium signaling pathway, such as Htr7, Gna14, Adra1a, Cysltr2, Itpr3, Ppp3cc, and Slc8a1, are central nodes in this network. The top core genes were chosen: Csf2, Fars2, Synj2, Ppp3cc, Stat4, Casp8, Cysltr2, and Tiel. These genes and

the number of gene cords are shown in Figure 4B. A total of 43 nodes and 33 interaction pairs were included in this network (Figure 4C). Some proteins involved in the Endocytosis pathway, such as Argef1, Flt1, Cyth1, Dnm3, Snx1, and Spg21, are central nodes in this network. The top core genes were chosen: Pcsk2, Dnm3, Hmgcll1, Flt1, Plcg2, RT1-Db1, Ntrk3, and Atp10a. These genes and the number of gene cords are shown in Figure 4D.

Genes expression validation by qRT-PCR

In addition to validating the WGBS analysis results, qRT-PCR was used to quantify parts of mRNAs of corresponding methylated genes in the SCI group compared with the sham group. Among these core genes, there were 5 differentially hypermethylated genes (Csf2, Fars2, Synj2, Ppp3cc, and Stat4) and 3 differentially hypomethylated genes (Pcsk2, Dnm3, and Hmgcll1). A search of PubMed revealed that all of these genes are involved in central nervous system repair. Figure 5 shows that 5 mRNAs of differentially hypermethylated genes were downregulated in the SCI group compared with the sham group ($P < 0.05$), and 3 mRNAs of differentially hypomethylated genes were upregulated in the SCI group compared with the sham group ($P < 0.05$).

Discussion

During the past decade, few studies have revealed the epigenetic changes that accompany the formation and development of the central nervous system [30,31]. In the early stages of the development of the central nervous system, DNA methylation may play an essential role. It is reported that DNA methylation regulates the differentiation of neurons, which is closely related to adult learning, memory, and cognition [32]. During the process of DNA methylation changes, it is easy to cause more epigenetic diseases due to other factors such as the environment. Therefore, whole-genome bisulfite sequencing of DNA methylation helps reveal epigenetic modifications underlying a variety of complex diseases.

In this study, we first established a transection model of spinal cord injury. Then, histological and motor function scores of Wistar rats before and after spinal cord injury were assessed. We further used whole-genome bisulfite sequencing to analyze

Table 3. Complete list of the 50 hypermethylated genes.

Chr	Symbol	ID	Length	Num. CpGs	DMR. p value	DMR. q value	Mean. meth. diff
chr10	Fbxw11	NM_001106993_I2_introns	13	3	3.97E-13	3.71E-11	41.39596773
chr1	Gna14	NM_001013151_I1_introns	44	3	4.18E-10	1.02E-08	39.78573567
chr2	Chi3l3	NM_001191712_I5_introns	289	3	6.72E-07	5.21E-06	39.31869094
chr1	Vps13a	NM_001100975_E54_exon	51	3	4.76E-10	1.07E-08	38.36766934
chr15	Adra1a	NM_017191_I1_introns	203	4	7.06E-13	2.54E-11	38.16288829
chr6	Frmd6	NM_001271054_I1_introns	171	3	7.03E-12	2.11E-10	37.4625921
chr7	Palm	NM_130829_I8_introns	170	4	0.000442034	0.001304001	36.40773047
chr6	Nubpl	NM_001185025_I4_introns	121	3	4.52E-07	6.02E-06	35.86094377
chr17	Crem	NM_001110860_I3_introns	105	3	8.12E-05	0.000517023	35.7757685
chr7	Fam227a	NM_001130581_I20_introns	61	3	0.000174069	0.000641881	35.64110942
chr10	Fstl4	NM_001107000_I4_introns	15	3	1.34E-05	0.000156783	34.86382548
chr2	Col11a1	NM_013117_I49_introns	226	3	1.04E-05	5.08E-05	34.8266253
chr10	Neurl1b	NM_001142652_I4_introns	80	7	9.05E-06	0.000120934	34.13727909
chr13	Plxna2	NM_001105988_I3_introns	219	3	3.78E-05	0.000184147	33.8264037
chr12	Fry	NM_001170398_I63_introns	55	4	8.19E-08	3.44E-06	33.49560871
chr10	Snx29	NM_001109526_I7_introns	6	4	2.56E-05	0.000217367	33.28848981
chr10	Litaf	NM_001105735_I1_introns	54	5	6.91E-10	2.59E-08	33.03121583
chr1	Slc22a3	NM_019230_I1_introns	28	3	3.77E-09	7.37E-08	33.00571733
chr18	Fbn2	NM_031826_I10_introns	202	4	1.04E-13	5.10E-12	32.59773088
chr17	Susd3	NM_001107341_I1_introns	228	4	5.87E-05	0.000435361	31.38181808
chr15	Cysltr2	NR_131894_I4_introns	390	4	0.000284111	0.000601647	30.97831867
chr15	Fndc3a	NM_001107278_I21_introns	516	5	0.000898606	0.001586244	30.17566608
chr2	Fat4	NM_001191705_I1_introns	449	5	2.40E-05	0.000101298	30.11072466
chr1	Syt3	NM_019122_I5_introns	71	3	2.07E-07	2.64E-06	29.85324558
chr18	Ldrad4	NM_001271365_I1_introns	85	3	0.000175281	0.00071573	29.56178745
chr19	Cdh13	NM_138889_I4_introns	116	10	7.40E-08	3.11E-06	29.18274327
chr10	Asic2	NM_001034014_I6_introns	11	4	0.000718251	0.002857722	28.85755303
chr1	Il4r	NM_133380_I1_introns	111	3	0.000835518	0.002523782	26.43736728
chr8	Kirrel3	NM_001048215_I1_introns	146	3	0.000935696	0.00519023	26.2257812
chr1	Ezr	NM_019357_I12_introns	86	13	3.17E-07	3.31E-06	25.69879184
chr2	Bank1	NM_001047918_I10_introns	696	6	0.000248188	0.000607409	25.27410866
chr15	Ppp3cc	NM_134367_I8_introns	628	3	1.49E-09	1.79E-08	25.22411799
chr10	Cpped1	NM_001013963_I3_introns	45	4	0.000373298	0.001745166	25.13311283
chr1	Ust	NM_001108458_I5_introns	138	3	2.52E-11	1.23E-09	25.06445554

Table 3 continued. Complete list of the 50 hypermethylated genes.

Chr	Symbol	ID	Length	Num. CpGs	DMR. p value	DMR. q value	Mean. meth. diff
chr9	Stat4	NM_001012226_I10_introns	125	3	6.22E-06	4.71E-05	24.88762551
chr10	Rab11fip4	NM_001107023_I3_introns	29	3	0.000195025	0.001022057	24.47716696
chr10	Dexi	NM_001109026_I1_introns	51	4	2.70E-09	6.48E-08	24.31882587
chr17	Mpp7	NM_001100575_I12_introns	128	3	0.000163608	0.000880968	24.29724306
chr10	Zc3h7a	NM_001108262_E23_exon	50	3	0.00033137	0.001621921	23.86498374
chr6	Slc8a1	NM_001270773_I6_introns	151	5	0.000633381	0.001794639	23.70245762
chr3	Tspan18	NM_001107750_I8_introns	41	3	0.000144543	0.00100661	23.25712602
chr1	Arntl	NM_024362_I2_introns	43	3	3.93E-14	2.88E-12	22.86236695
chr15	Ppp2r2a	NM_053999_I7_introns	205	15	7.78E-09	5.60E-08	22.86049685
chr2	Arsb	NM_033443_I4_introns	1282	21	5.69E-14	2.65E-12	22.42210761
chr5	Slco5a1	NM_001107898_I8_introns	154	4	0.000156566	0.0007552	22.36790713
chr8	Arhgap20	NM_213629_I9_introns	59	5	0.000990502	0.00519023	21.72558987
chr6	Arid4a	NM_001108029_I5_introns	100	4	0.00047549	0.00142647	21.4264141
chr1	Syt17	NM_138849_I3_introns	56	3	1.50E-05	6.87E-05	21.27406378
chr1	Sym	NM_001134858_I2_introns	104	5	9.91E-07	8.06E-06	21.19753403
chr6	Rtn1	NM_053865_I49_introns	141	3	4.75E-05	0.000195013	21.15397951

Table 4. Complete list of the 46 hypomethylated genes.

Chr	Symbol	ID	Length	Num. CpGs	DMR. p value	DMR. q value	Mean. meth. diff
chr8	Snx1	NM_053411_I8_introns	16	3	0.000178924	0.001674221	39.23422802
chr10	Nubp1	NM_001009619_I9_introns	51	3	2.77E-09	6.48E-08	38.19511889
chr19	Atp6v0d1	NM_001011927_I7_introns	27	3	8.97E-07	1.88E-05	37.45568608
chr8	Bckdhb	NM_019267_I3_introns	91	6	4.56E-11	1.99E-09	36.09637024
chr6	Prkch	NM_031085_I10_introns	130	4	5.03E-06	3.02E-05	35.65709264
chr13	Hmcn1	NM_001271292_I106_introns	168	3	4.14E-08	4.04E-07	35.19645258
chr1	Zp2	NM_031150_E10_exon	79	4	0.00049086	0.001580462	33.48819301
chr2	Ptpn22	NM_001106460_I13_introns	70	3	5.71E-05	0.000202829	32.53343885
chr2	Skiv2l2	NM_001034093_I2_introns	95	4	3.00E-08	3.49E-07	31.5071179
chr1	Tulp2	NM_001012168_I1_introns	110	6	9.46E-07	7.92E-06	31.18947695
chr12	Fry	NM_001170398_I14_introns	19	3	2.19E-05	0.000288601	30.41340002
chr1	Slco3a1	NM_177481_I8_introns	85	3	0.000528807	0.001684136	30.13666411
chr1	Atp10a	NM_001141935_I3_introns	27	6	1.03E-06	8.14E-06	30.06814676
chr1	Prkg1	NM_001105731_I15_introns	70	5	0.000356284	0.001186265	28.94112061
chr4	Grm7	NM_031040_I7_introns	192	3	0.000245364	0.001003763	28.53745911

Table 4. Complete list of the 46 hypomethylated genes.

Chr	Symbol	ID	Length	Num. CpGs	DMR. p value	DMR. q value	Mean. meth. diff
chr10	Carhsp1	NM_152790_I2_introns	102	5	2.26E-05	0.000211468	28.25784027
chr2	Noct	NM_138526_I1_introns	17	3	0.000373085	0.000889665	28.10593157
chr15	Gpc5	NM_001107285_I2_introns	205	4	2.72E-09	2.44E-08	27.84298084
chr16	Nrg1	NM_001271130_I1_introns	272	4	0.000226123	0.000621838	27.46776641
chr7	Dmc1	NM_001130567_I6_introns	134	3	0.000623225	0.001671375	27.18046865
chr8	Tex264	NM_001007665_I3_introns	13	4	4.67E-12	3.06E-10	26.94493645
chr1	Oprm1	NR_027877_I3_introns	167	4	5.98E-05	0.000236705	26.39509712
chr1	Ntrk3	NM_001270655_I14_introns	19	4	0.000915163	0.00273615	26.34513213
chr6	Psmal1	NM_001004094_I5_introns	128	3	1.84E-06	1.57E-05	26.13483738
chr6	Psmal3	NM_017280_I5_introns	128	3	1.84E-06	1.57E-05	26.13483738
chr7	Cpq	NM_031640_I8_introns	174	5	0.000464492	0.001305002	25.03471249
chr1	Tpd52l1	NM_001044295_I1_introns	43	4	2.22E-06	1.41E-05	24.99670494
chr1	RGD1307603	NM_001134508_E3_exon	35	6	6.18E-05	0.000241568	24.98945466
chr19	Gfod2	NM_001107421_I2_introns	100	9	4.56E-06	6.38E-05	24.49436882
chr10	Cyth1	NM_053910_E12_exon	56	6	2.55E-05	0.000217367	24.45542274
chr13	Gpatch2	NM_001011909_I1_introns	258	3	9.48E-05	0.000369638	23.92339964
chr9	Myo1b	NM_053986_I3_introns	136	6	8.64E-05	0.000351935	23.4475614
chr18	Ldlrad4	NM_001271365_I5_introns	494	14	5.50E-07	5.39E-06	23.43565697
chr6	Frmd6	NM_001271054_I1_introns	304	4	0.000701646	0.001871057	23.28083922
chr1	Plpp4	NM_001191631_I5_introns	86	3	1.05E-05	5.31E-05	23.22492261
chr1	Gpr139	NM_001024241_I1_introns	38	3	0.00021821	0.000752181	22.95290692
chr10	Ccdc40	NM_001134688_I1_introns	38	4	4.16E-05	0.000338144	22.84818656
chr13	Cntnap5b	NM_001047873_I1_introns	329	3	1.10E-05	6.16E-05	22.56555396
chr19	Zfp612	NM_001107428_I3_introns	169	5	0.000905479	0.004444048	22.51841655
chr8	Dpp8	NM_001108159_I13_introns	120	13	0.000326038	0.002512407	22.4358468
chr9	Sphkap	NM_001127492_I13_introns	199	4	0.000143173	0.000508033	21.12261507
chr1	Ipcef1	NM_001170799_I1_introns	88	4	0.000961996	0.002847121	20.82969003
chr5	Slco5a1	NM_001107898_I1_introns	62	3	8.67E-05	0.000473983	20.47392161
chr4	Prickle2	NM_001107876_I1_introns	181	7	0.000537784	0.001861562	20.45460701
chr1	Hddc2	NM_001108460_I2_introns	61	4	2.61E-05	0.000112648	20.32430339
chr9	Kcnh8	NM_145095_I9_introns	302	5	3.28E-05	0.000150472	20.01509207

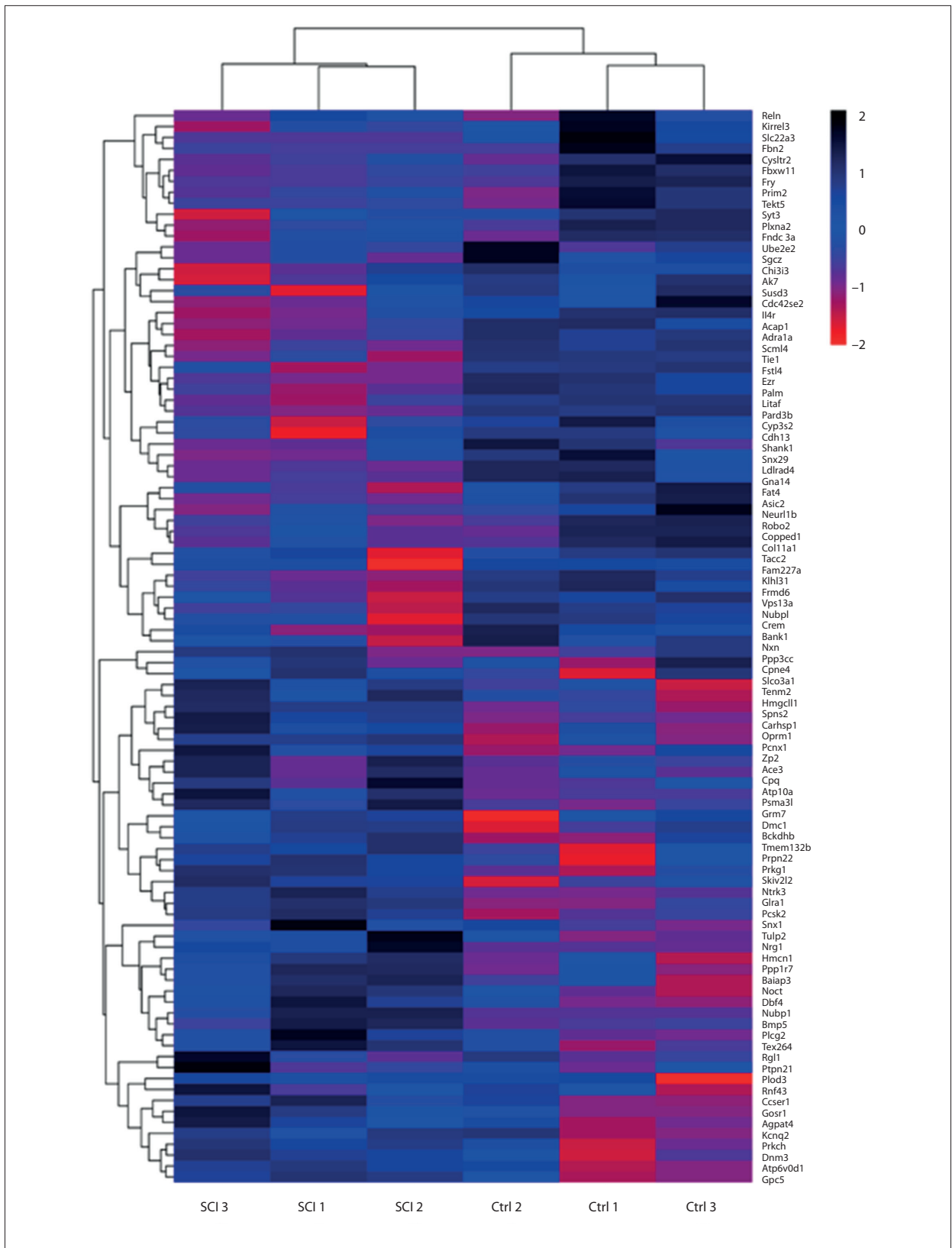


Figure 3. Representative heat map of the top 100 differentially methylated genes. Red indicates hypermethylated genes and blue indicates hypomethylated genes.

Table 5. Gene ontology analysis of aberrantly methylated-differentially expressed genes in spinal cord injury.

Category	Term	Count	%	P value
GOTERM_BP_DIRECT	GO:0007283 spermatogenesis	6	5	0.083899175
GOTERM_BP_DIRECT	GO:0008360 regulation of cell shape	5	4.1	0.007915904
GOTERM_BP_DIRECT	GO:0022008 neurogenesis	4	3.3	0.00873703
GOTERM_BP_DIRECT	GO:0006470 protein dephosphorylation	4	3.3	0.032688039
GOTERM_BP_DIRECT	GO:0006897 endocytosis	4	3.3	0.046516317
GOTERM_CC_DIRECT	GO:0005886~plasma membrane	33	0.2	0.035034848
GOTERM_CC_DIRECT	GO:0070062~extracellular exosome	27	0.1	0.005859253
GOTERM_CC_DIRECT	GO:0016020~membrane	22	0.1	0.018591495
GOTERM_CC_DIRECT	GO:0005887~integral component of plasma membrane	14	0.1	0.003864181
GOTERM_CC_DIRECT	GO:0048471~perinuclear region of cytoplasm	13	0.1	0.000430891
GOTERM_MF_DIRECT	GO:0005515~protein binding	19	0.1	0.005508607
GOTERM_MF_DIRECT	GO:0046872~metal ion binding	15	0.1	0.032965821
GOTERM_MF_DIRECT	GO:0005509~calcium ion binding	12	0.1	0.002804787
GOTERM_BP_DIRECT	GO:0007420~brain development	8	6.1	0.00348475
GOTERM_BP_DIRECT	GO:0006468~protein phosphorylation	8	6.1	0.043342319
GOTERM_BP_DIRECT	GO:0045471~response to ethanol	6	4.6	0.008263832
GOTERM_BP_DIRECT	GO:0007399~nervous system development	6	4.6	0.009359172
GOTERM_BP_DIRECT	GO:0007613~memory	5	3.8	0.002955411
GOTERM_CC_DIRECT	GO:0005737~cytoplasm	46	35.1	0.023089945
GOTERM_CC_DIRECT	GO:0070062~extracellular exosome	34	26	0.00016196
GOTERM_CC_DIRECT	GO:0016020~membrane	21	16	0.084368826
GOTERM_CC_DIRECT	GO:0005829~cytosol	18	13.7	0.031630643
GOTERM_CC_DIRECT	GO:0005887~integral component of plasma membrane	15	11.5	0.003637411
GOTERM_MF_DIRECT	GO:0005515~protein binding	22	16.8	0.001727352
GOTERM_MF_DIRECT	GO:0005509~calcium ion binding	10	7.6	0.042887314
GOTERM_MF_DIRECT	GO:0042803~protein homodimerization activity	10	7.6	0.088758008
GOTERM_MF_DIRECT	GO:0030165~PDZ domain binding	4	3.1	0.043421165
GOTERM_MF_DIRECT	GO:0005516~calmodulin binding	4	3.1	0.08759155

epigenetic changes in rat spinal cords before and after injury. In bioinformatics analysis, approximately 96 differential DNA methylation genes were identified, including 50 hypermethylation genes and 46 hypomethylated genes. After GO enrichment analysis, KEGG signaling pathway analysis, and PPI network analysis of these significantly different DNA methylated genes, several core genes in this epigenetic change were screened out, such as *Csf2*, *Fars2*, *Synj2*, *Ppp3cc*, *Stat4*, *Pcsk2*,

Dnm3, and *Hmgcll1*. In addition, we used qRT-PCR to verify the expression of these genes.

Bioinformatics analysis was performed on the selected hypomethylated genes. In GO analysis of biological processes, these hypomethylated genes were significantly enriched in brain development, protein phosphorylation, and response to ethanol, while in the cellular component, the hypomethylated genes

Table 6. KEGG pathway analysis of aberrantly methylated-differentially expressed genes in spinal cord injury.

Pathway name	Gene num	P-value	Genes
Hypermethylation			
Calcium signaling pathway	7	0.001367652	Htr7, Gna14, Adra1a, Cysltr2, Itpr3, Ppp3cc, Slc8a1
Endocytosis pathway	6	0.041783996	Acap1, Ehd4, Rab11fip4, Sh3kbp1, Smurf1, Dnm3
T cell receptor signaling pathway	4	0.020396716	Csf2, Ctla4, Ppp3cc, Vav2
Axon guidance	4	0.053653812	Dpysl2, Plxna2, Ppp3cc, Robo2
Dopaminergic synapse	4	0.054679627	Arntl, Itpr3, Ppp2r2a, Ppp3cc
Taste transduction	3	0.053663995	Asic2, Itpr3, Trpm5
Hypomethylation			
Endocytosis pathway	6	0.041783996	Arfgef1, Flt1, Cyth1, Dnm3, Snx1, Spg21
Hippo signaling pathway	4	0.082043834	Frmd6, Bmp5, Ctnna2, Dlg2

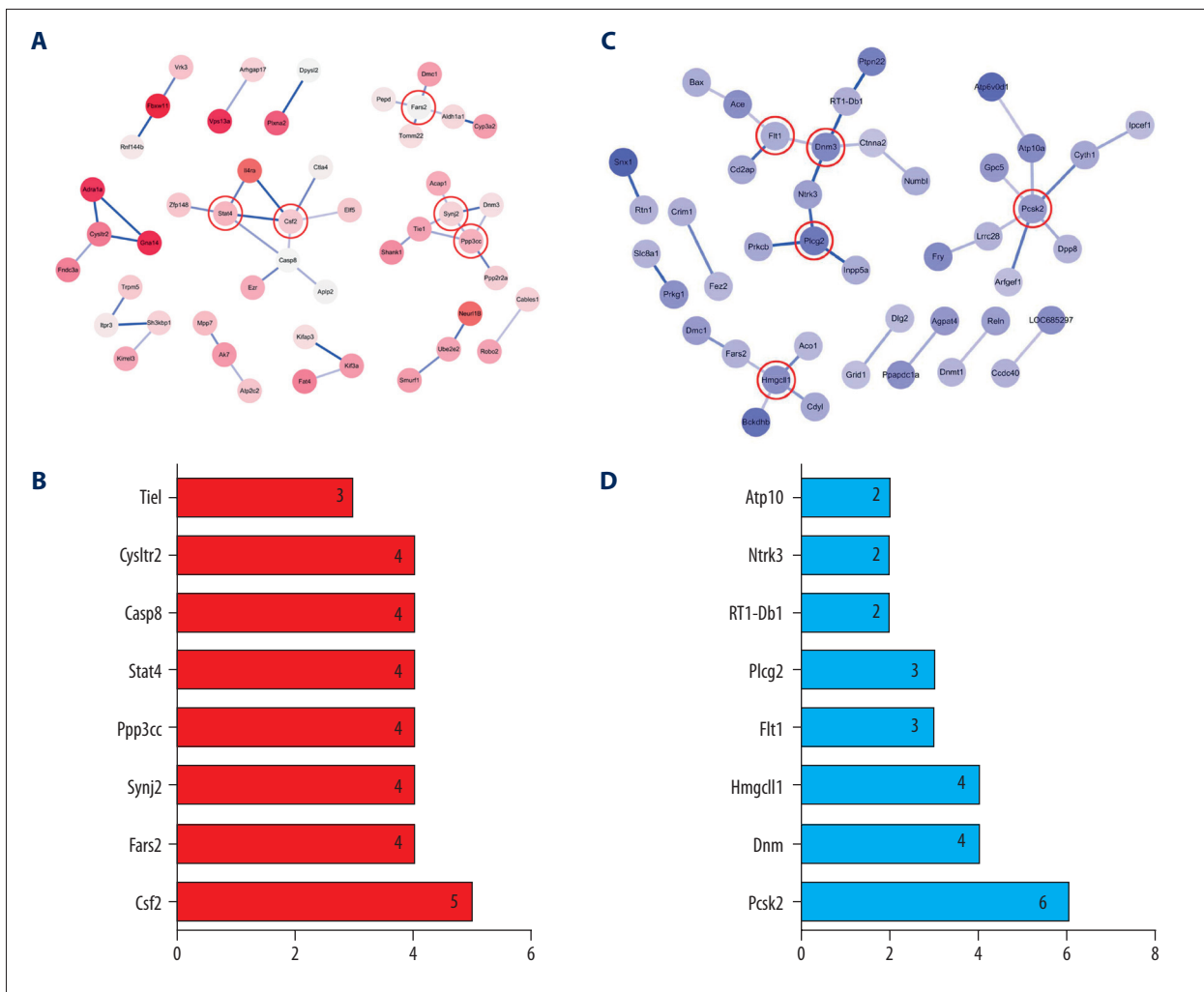


Figure 4. PPI network and the Core genes. (A) PPI network of hypermethylated genes. (B) Core genes of hypermethylated genes. (C) PPI network of hypomethylated genes. (D) Core genes of hypomethylated genes.

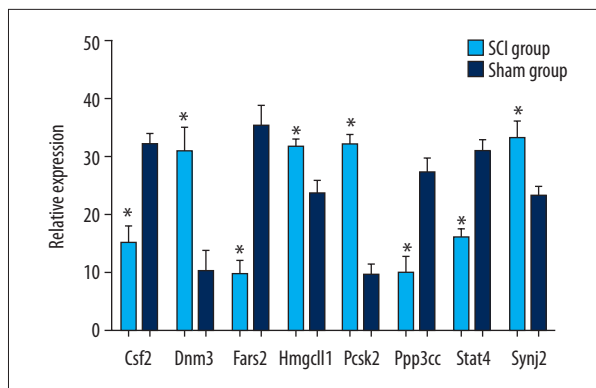


Figure 5. Validation of the differential expression of 8 mRNAs of corresponding methylated genes identified in the WGBS in the SCl group compared with the sham group by qRT-PCR. Values are means \pm SE (* $P < 0.05$).

were enriched in cytoplasm and extracellular exosome. These hypomethylated genes may be closely related to the formation and regeneration of the central nervous system, and epigenetic changes in these genes may lead to the proliferation and migration of nerve cells (e.g., neurons, oligodendrocytes, and astrocytes) after nerve injury. Among these genes, Dnm3 attracted our attention. Previous reports have shown that Dnm3 is an important epigenetic marker for early detection of breast cancer [33]. There is increasing evidence that Dnm3 plays a critical role in primordial short stature, neurodevelopmental impairments, and microcephaly [34]. In addition, Dnm3 is expressed in the brain and contributes to myelin formation, which promotes axon maturation and myelination [35–36]. This is consistent with changes in hypomethylated genes affecting axonal remodeling after spinal cord injury in rats in the present study. In KEGG analysis, these hypomethylated genes were significantly enriched in the Endocytosis pathway and Hippo signaling pathway. This may be related to the influence of Dnm3 on the coupling between the post-synaptic density scaffold and the endocytic zones [37]. Previous studies have shown that the use of a proliferation-inducing medium containing Y-27632 (Rho/Rho-kinase pathway inhibitor) to culture neural stem cells (NSCs) can activate the Hippo signaling pathway and enhance axon regeneration of NSCs [38], and found that inhibition of ROCK mediates neurite outgrowth in NSCs by activating the Hippo signaling pathway. This is consistent with the results of the present study. After PPI analysis of the hypomethylated genes, the top 5 core genes were Pcsk2, Dnm3, Hmgcll1, Flt1, and Plcg2.

In GO analysis, we found that the hypermethylated genes enriched in biological processes included spermatogenesis, neurogenesis, and regulation of cell shape. In molecular function, the hypermethylated genes were mainly enriched in metal ion binding and plasma protein binding. Regarding the cellular component, we found the hypermethylated genes were

significantly enriched in membrane, extracellular exosome, and membrane. Csf2 is a member of the colony-stimulating factors (CSFs) family. This cytokine family includes widely known hematopoietic growth factors [39,40]. Initially, colony-stimulating factor 2 was reported to play a key role in embryonic and early nervous system development [41]. A previous study focused on long noncoding RNAs and messenger RNAs indicated that Csf2 contributes to pathogenesis in the immediate phase of spinal cord injury in adult SD rats [42]. These results all suggest that Csf2 genes may be potential biomarkers in the central nervous system. KEGG analysis showed that these hypermethylated genes were significantly enriched in the T cell receptor signaling pathway, Axon guidance pathway, Calcium signaling pathway, Dopaminergic synapse pathway, and Taste transduction pathway. Previous research has indicated that T cell receptor signaling pathways are crucial in development of neuropathic pain following spinal cord injury [43]. Another study demonstrated that changes in the Axon guidance pathway along with an upregulation of voltage-dependent calcium channel alpha (2) delta-1 subunit *Cacna2d1*, could contribute to increased mechanical sensitivity [44]. These pathway changes are consistent with the results of our study. In addition, we performed PPI network analysis on hypermethylated genes; the top 5 core genes were Csf2, Fars2, Synj2, Ppp3cc, and Stat4.

Although this study is the first to reveal epigenetic changes after spinal cord injury in Wistar rats, there are still some limitations that need to be addressed. First, we used rodent models, and primate models and even human studies are needed. Second, the central nervous system contains the spinal cord and brain, and the structure and function of the brain are more complex than in the spinal cord, but we did not perform epigenetic studies of the brain. Third, DNA methylation is an important part of epigenetics, and after spinal cord injury, histone modification, gene silencing, and changes in genomic imprinting need to be further explored. In addition, the type of spinal cord injury should be assessed and the screening of more core genes is needed in future work. Despite these limitations, this study furthers understanding of epigenetic changes in spinal cord injury.

Conclusions

The present study performed a comprehensive bioinformatics analysis; 96 differential DNA methylation genes were identified in the thoracic spinal cord tissue following transection injury compared with sham group samples. Among them, 50 genes were hypermethylated and 46 genes were hypomethylated. Moreover, the Axon guidance pathway, Endocytosis pathway, T cell receptor signaling pathway, and Hippo signaling pathway were identified and may be significant mechanisms involved. Core genes such as Csf2, Fars2, Synj2, Ppp3cc, Stat4, Pcsk2,

Dnm3, and Hmgcll1 are potential new markers for more accurate diagnosis and effective therapy of spinal cord injury. These markers can be used in drug therapy to alleviate the development of neuropathic pain caused by spinal cord injury and to promote axon maturation, myelin formation, and nerve repair.

References:

- Anderson MA, Burda JE, Ren Y et al: Astrocyte scar formation aids central nervous system axon regeneration. *Nature*, 2016; 532(7598): 195–200
- Assinck P, Duncan GJ, Hilton BJ et al: Cell transplantation therapy for spinal cord injury. *Nat Neurosci*, 2017; 20(5): 637–47
- Rodrigues LF, Moura-Neto V, E Spohr TCLS: Biomarkers in spinal cord injury: From prognosis to treatment. *Mol Neurobiol*, 2018; 55(8): 6436–48
- Nees TA, Finnerup NB, Blesch A, Weidner N: Neuropathic pain after spinal cord injury: The impact of sensorimotor activity. *Pain*, 2017; 158(3): 371–76
- Fan B, Wei Z, Yao X et al: Microenvironment imbalance of spinal cord injury. *Cell Transplant*, 2018; 27(6): 853–66
- Becker CG, Becker T, Hugnot JP: The spinal ependymal zone as a source of endogenous repair cells across vertebrates. *Prog Neurobiol*, 2018; 170: 67–80
- Zhou X, Shi G, Fan B et al: Polycaprolactone electrospun fiber scaffold loaded with iPSCs-NSCs and ASCs as a novel tissue engineering scaffold for the treatment of spinal cord injury. *Int J Nanomedicine*, 2018; 13: 6265–77
- Niclis JC, Turner C, Durnall J et al: Long-distance axonal growth and protracted functional maturation of neurons derived from human induced pluripotent stem cells after intracerebral transplantation. *Stem Cells Transl Med*, 2017; 6(6): 1547–56
- Waddington CH: Canalization of development and genetic assimilation of acquired characters. *Nature*, 1959; 183(4676): 1654–55
- Waddington CH: The epigenotype. 1942. *Int J Epidemiol*, 2012; 41(1): 10–13
- Bird A: DNA methylation patterns and epigenetic memory. *Genes Dev*, 2002; 16(1): 6–21
- Margueron R, Trojer P, Reinberg D: The key to development: interpreting the histone code? *Curr Opin Genet Dev*, 2005; 15(2): 163–76
- Gould E: How widespread is adult neurogenesis in mammals? *Na Rev Neurosci*, 2007; 8(6): 481–88
- Ming GL, Song H: Adult neurogenesis in the mammalian brain: Significant answers and significant questions. *Neuron*, 2011; 70(4): 687–702
- Nwaobi SE, Lin E, Peramsetty SR, Olsen ML: DNA methylation functions as a critical regulator of Kir4.1 expression during CNS development. *Glia*, 2014; 62(3): 411–27
- Blaze J, Wang J, Ho L et al: Polyphenolic compounds alter stress-induced patterns of global DNA methylation in brain and blood. *Mol Nutr Food Res*, 2018; 62(8): e1700722
- Losi L, Fonda S, Saponaro S et al: Distinct DNA methylation profiles in ovarian tumors: Opportunities for novel biomarkers. *Int J Mol Sci*, 2018; 19(6): pii: E1559
- Nicolia V, Cavallaro RA, Lopez-Gonzalez I et al: DNA methylation profiles of selected pro-inflammatory cytokines in Alzheimer disease. *J Neuropathol Exp Neurol*, 2017; 76(1): 27–31
- Miyake K, Kawaguchi A, Miura R et al: Association between DNA methylation in cord blood and maternal smoking: The Hokkaido Study on Environment and Children's Health. *Sci Rep*, 2018; 8(1): 5654
- Capper D, Jones DTW, Sill M et al: DNA methylation-based classification of central nervous system tumours. *Nature*, 2018; 555(7697): 469–74
- Du BL, Zeng X, Ma YH et al: Graft of the gelatin sponge scaffold containing genetically-modified neural stem cells promotes cell differentiation, axon regeneration, and functional recovery in rat with spinal cord transection. *J Biomed Mater Res A*, 2015; 103(4): 1533–45
- Lai BQ, Wang JM, Ling EA et al: Graft of a tissue-engineered neural scaffold serves as a promising strategy to restore myelination after rat spinal cord transection. *Stem Cells Dev*, 2014; 23(8): 910–21
- Lu P, Woodruff G, Wang Y et al: Long-distance axonal growth from human induced pluripotent stem cells after spinal cord injury. *Neuron*, 2014; 83(4): 789–96
- Shannon P, Markiel A, Ozier O et al: Cytoscape: A software environment for integrated models of biomolecular interaction networks. *Genome Res*, 2003; 13(11): 2498–504
- Li S, Garrett-Bakelman FE, Akalin A et al: An optimized algorithm for detecting and annotating regional differential methylation. *BMC Bioinformatics*, 2013; 14(Suppl. 5): S10
- Dennis G Jr., Sherman BT, Hosack DA et al: DAVID: Database for annotation, visualization, and integrated discovery. *Genome Biol*, 2003; 4(5): P3
- Li G, Cao Y, Shen F et al: Mdivi-1 inhibits astrocyte activation and astroglial scar formation and enhances axonal regeneration after spinal cord injury in rats. *Front Cell Neurosci*, 2016; 10: 241
- Zhao L, Wang Q, Zhang C, Huang C: Genome-wide DNA methylation analysis of articular chondrocytes identifies TRAF1, CTGF, and CX3CL1 genes as hypomethylated in osteoarthritis. *Clin Rheumatol*, 2017; 36(10): 2335–42
- Basso DM, Beattie MS, Bresnahan JC: A sensitive and reliable locomotor rating scale for open field testing in rats. *J Neurotrauma*, 1995; 12(1): 1–21
- Aiba T, Saito T, Hayashi A et al: Does the prenatal bisphenol A exposure alter DNA methylation levels in the mouse hippocampus?: An analysis using a high-sensitivity methylome technique. *Genes Environ*, 2018; 40: 12
- Li X, Xiao B, Chen XS: DNA methylation: A new player in multiple sclerosis. *Mol Neurobiol*, 2017; 54(6): 4049–59
- Huang WQ, Yi KH, Li Z et al: DNA methylation profiling reveals the change of inflammation-associated ZC3H12D in leukoaraiosis. *Front Aging Neurosci*, 2018; 10: 143
- Uehiro N, Sato F, Pu F et al: Circulating cell-free DNA-based epigenetic assay can detect early breast cancer. *Breast Cancer Res*, 2016; 18(1): 129
- Burkhardt DD, Rosenfeld JA, Helgeson ML et al: Distinctive phenotype in 9 patients with deletion of chromosome 1q24-q25. *Am J Med Genet A*, 2011; 155A(6): 1336–51
- Sala C, Piëch V, Wilson NR et al: Regulation of dendritic spine morphology and synaptic function by Shank and Homer. *Neuron*, 2001; 31(1): 115–30
- Jahn O, Tenzer S, Werner HB: Myelin proteomics: molecular anatomy of an insulating sheath. *Mol Neurobiol*, 2009; 40(1): 55–72
- Lu J, Helton TD, Blanpied TA et al: Postsynaptic positioning of endocytic zones and AMPA receptor cycling by physical coupling of dynamin-3 to Homer. *Neuron*, 2007; 55(6): 874–89
- Jia XF, Ye F, Wang YB, Feng DX: ROCK inhibition enhances neurite outgrowth in neural stem cells by upregulating YAP expression *in vitro*. *Neural Regen Res*, 2016; 11(6): 983–87
- Robertson SA: GM-CSF regulation of embryo development and pregnancy. *Cytokine Growth Factor Rev*, 2007; 18(3–4): 287–98
- Sferruzzi-Perri AN, Macpherson AM, Roberts CT, Robertson SA: Csf2 null mutation alters placental gene expression and trophoblast glycogen cell and giant cell abundance in mice. *Biol Reprod*, 2009; 81(1): 207–21
- Smith A, Witte E, McGee D et al: Cortisol inhibits CSF2 and CSF3 via DNA methylation and inhibits invasion in first-trimester trophoblast cells. *Am J Reprod Immunol*, 2017; 78(5)
- Zhou H, Shi Z, Kang Y et al: Investigation of candidate long noncoding RNAs and messenger RNAs in the immediate phase of spinal cord injury based on gene expression profiles. *Gene*, 2018; 661: 119–25
- He X, Fan L, Wu Z et al: Gene expression profiles reveal key pathways and genes associated with neuropathic pain in patients with spinal cord injury. *Mol Med Rep*, 2017; 15(4): 2120–28
- Capasso KE, Manners MT, Quershi RA et al: Effect of histone deacetylase inhibitor jnj-26481585 in pain. *J Mol Neurosci*, 2014; 55(3): 570–78

Conflicts of Interest

None.